Available online at www.sciencedirect.com
ScienceDirect
Journal of the European Ceramic Society 27 (2007) 3331–3337
www.elsevier.com/locate/jeurceramsoc

Transparent yttrium aluminum garnet (YAG) ceramics by spark plasma sintering

Rachman Chaim [a,*], Michael Kalina [a], James Z. Shen [b]

[a] *Department of Materials Engineering, Technion-Israel Institute of Technology, Haifa 32000, Israel*
[b] *Department of Inorganic Chemistry, Arrhenius Laboratory, Stockholm University, S-10691 Stockholm, Sweden*

Available online 26 April 2007

Abstract

Commercial nanocrystalline yttrium aluminum garnet (nc-YAG) powders were used for fabrication of dense and transparent YAG by spark plasma sintering (SPS). Spherical 34 nm size particles were densified by SPS between 1200 and 1500 °C using 50 and 100 MPa pressures for 3, 6, and 9 min durations. Fully dense and transparent polycrystalline cubic YAG with micrometer grain size were fabricated at very moderate SPS conditions, i.e. 1375 °C, 100 MPa for 3 min. Increase in the SPS duration and pressure significantly increased the density especially at the lower temperature range. The observed microstructure is in agreement with densification by nano-grain rotation and sliding at lower densities, followed by curvature driven grain boundary migration and normal grain growth at higher densities. Residual nanosize pores at the grain boundary junctions are an inherent microstructure feature due to the SPS process.

Keywords: Grain growth; Hot pressing; Optical properties; Spark plasma sintering

1. Introduction

Optically transparent ceramics are often single crystals formed by the crystal growth techniques. Densification of polycrystalline ceramics to optical transparency in the visible range is yet a challenge and necessitates prolong sintering at very high temperatures under high vacuum conditions.[1,2] Recently, spark plasma sintering (SPS) was used for rapid densification of translucent and transparent functional[3,4] and nanocrystalline[5] (nc) ceramics. In the later study, 40% transmittance was measured in nc-MgO specimens densified by SPS for 5 min at 800 °C and 150 MPa. The extraordinary densification rate was achieved at temperatures as low as $0.34T_m$; T_m being the melting point of MgO in Kelvin. For comparison, fabrication of transparent polycrystalline MgO necessitates temperatures as high as 1600 °C (i.e. $0.6T_m$) for prolong durations using sintering additives.[6] Likewise, extremely high temperatures, close to the melting point were required for vacuum sintering of yttrium aluminum garnet (YAG) to transparency.[7–9] In this respect, fast fabrication of fully dense, transparent polycrystalline optic and optoelectronic ceramic oxides, such as YAG, yttrium oxide, aluminum magnesium spinel ($MgAl_2O_4$) and others is of prime importance both scientifically and commercially due to their diverse mechanical and physical properties. However, as was shown by the theoretical calculations, fast and low-temperature densification of green compacts by SPS necessitates powder compacts with a nanocrystalline character, without which full densification to transparency may not be possible.[10,11] Therefore, the feasibility of the SPS for fabrication of fully dense, transparent polycrystalline YAG ceramics was investigated in the present study. This paper describes the overall microstructure and process aspects of the nc-YAG powder compacts densified at different SPS conditions.

2. Experimental procedures

Commercial nanocrystalline YAG powder (Tal Materials Inc.) fabricated by flame spraying[12] was used. Based on the dilatometric shrinkage behaviour of the cold isostatically pressed (CIP) powder compact, different temperatures, pressures, and durations were used for the SPS experiments as summarized in Table 1. The SPS experiments were performed in a SPS apparatus, Dr. Sinter 2050 in Stockholm (Sumitomo Coal Mining Co. Ltd., Japan) in vacuum using the graphite dies. Generally, measured quantity of the as-received powder was poured into the die with an inner diameter of 12 mm. Graphite foils (Grafoil) were used as spacers between the specimen and

* Corresponding author. Tel.: +972 4 829 4589; fax: +972 4 829 5677.
E-mail address: rchaim@technion.ac.il (R. Chaim).

0955-2219/$ – see front matter © 2007 Elsevier Ltd. All rights reserved.
doi:10.1016/j.jeurceramsoc.2007.02.193

Table 1
SPS parameters used for the nc-YAG powder

Specimen no.	SPS conditions temp./time/pressure	Density (g/cm^3)	Relative density (%)[a]	Appearance
Main runs				
1	1250/3/100	3.7903	83.24	White, Opaque
2	1300/3/100	4.0426	88.78	White, Opaque
3	1350/3/100	4.4319	97.33	White, Opaque
4	1400/3/100	4.5282	99.45	Transparent, core/shell
5	1450/3/100	4.5243	99.36	Transparent, core/shell
6	1500/3/100	4.5282	99.45	Transluscent
Time was doubled				
7	1200/6/100	3.9146	85.97	White, Opaque
8	1300/6/100	4.4567	97.88	White, Opaque
9	1350/6/100	4.4853	98.50	Transparent, core/shell
10	1375/6/100	4.4844	98.48	Transparent, homogeneous
11	1400/6/100	4.5170	99.20	Transluscent
12	1500/6/100	4.5262	99.40	Transluscent
Lower load				
13	1350/3/50	3.9928	87.69	White, Opaque
14	1400/3/50	4.4782	98.35	Transparent, homogeneous
Time was tripled				
15	1350/9/100	4.4977	98.78	Transparent, homogeneous

[a] Theoretical density 4.5533 g cm^{-3}.

the graphite die and punches. This set-up was pre-pressed to 100 MPa before heating. The pressure was maintained during the heating and at the SPS temperature for the SPS duration. The temperature was increased to 600 °C within 3 min, after which the heating rate of 100 °C/min was applied. The temperature was monitored using both thermocouple and optical pyrometer. The pressure was released when the cooling started from the SPS temperature.

The typical relative green density of these nc-YAG powders compacted by cold isostatic pressing under 100 MPa pressure is ~50%. The densities were determined at each stage by weighing and the Archimedes technique. Selected specimens were polished down to 0.25 μm using a diamond paste; the transparency of these specimens was determined by in-line transmission measurements within the visible range.

The microstructure of the sintered specimens was characterized using high resolution scanning electron microscopy (HRSEM, LEO Gemini 982), transmission electron microscopy (TEM, Jeol 2000FX), and X-ray diffraction (XRD, PW 1820). The specimens for the different examinations were prepared by the conventional techniques.

3. Results

3.1. Powder characteristics

The nc-YAG powder was consisted of non-agglomerated spherical shape particles (Fig. 1a) with 34 ± 17 nm average particle diameter, and log-normal particle size distribution (Fig. 1b). The powder particles were examined both by XRD and electron diffraction within TEM, exhibited a mixture of amorphous and crystalline nano-particles with cubic symmetry (Fig. 2).

In order to determine the temperature window for the SPS experiments, cylindrical powder compacts were CIPed at 240 MPa and used in dilatometer, the linear shrinkage curve of which is shown in Fig. 3. Although the main macroscopic shrinkage occurs around 1400 °C (Fig. 3a) the actual shrinkage starts already at 1130 °C (arrowed in Fig. 3b) and corresponds to the temperature at which the sintering shrinkage dominates over the thermal expansion. Therefore, the temperature range of 1200–1500 °C was used for the SPS, while changing parameters such as SPS duration (3–9 min) and pressure (halved from 100 to 50 MPa) (Table 1). One specimen was sintered for 3 min at 900 °C and further annealed for 5 h at 900 °C to check the homogeneity of the green microstructure.

3.2. Densification and grain growth

Densification of nanocrystalline powder compacts by cold pressing is commonly associated with entrapment of large pores, relative to the particle size, due to the agglomerating nature of the powder. The closure of such pores during pressureless sintering and densification may be very hard, if not impossible, due to the high dihedral angles at the pore-grain boundary junctions. The homogeneous distribution of the particles and the pores with comparable size found in the SPS compact at 900 °C (Fig. 4) points to the non-agglomerating character of the nc-YAG powder. Nevertheless, the homogeneous and small pore size observed in this partially sintered specimen (Fig. 4b) can not lead to full densification by the pressureless sintering since many pores with high coordination numbers (i.e. >6 in 2D) exist and thus cannot be annealed out. However pressure assisted sintering by SPS may assist the closure of such pores by grain sliding. The grain size distribution in

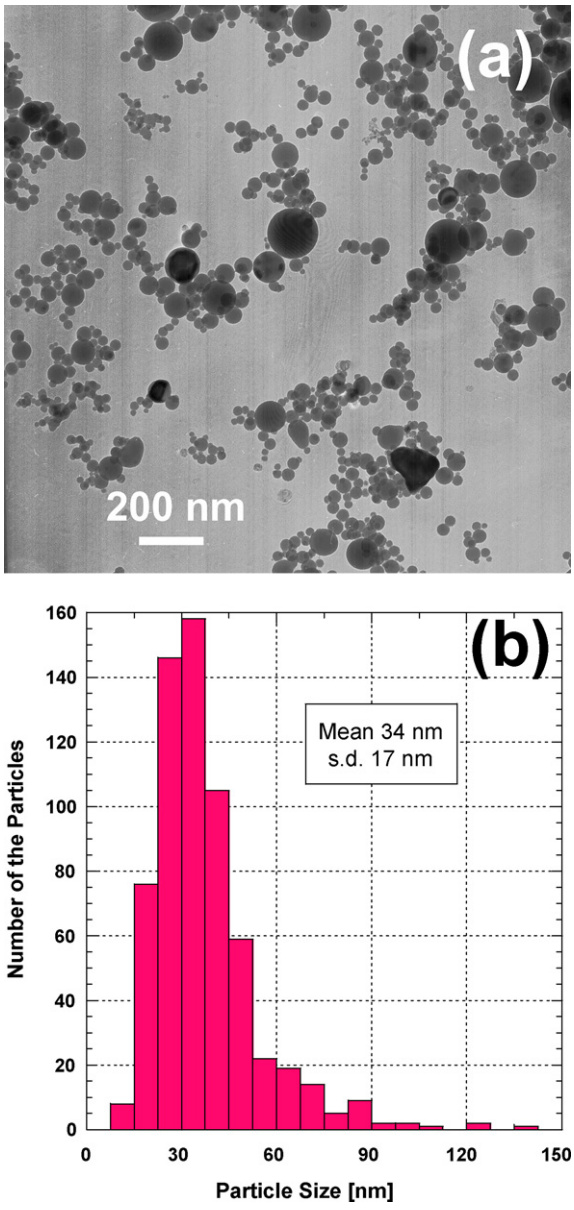

Fig. 1. (a) Bright field TEM image of the flame sprayed nc-YAG spherical powder and (b) its corresponding particle size distribution with log-normal character and average particle diameter of 34 ± 17 nm.

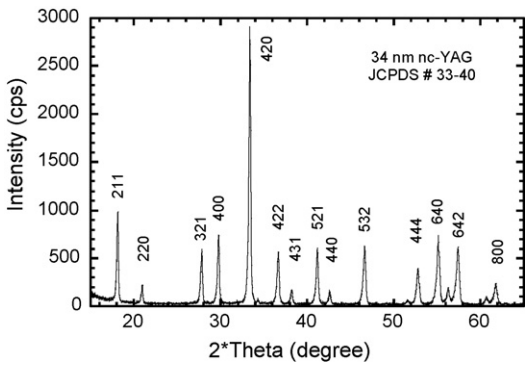

Fig. 2. X-ray diffraction spectrum from the nc-YAG powder showing the cubic symmetry of the nanocrystalline particles.

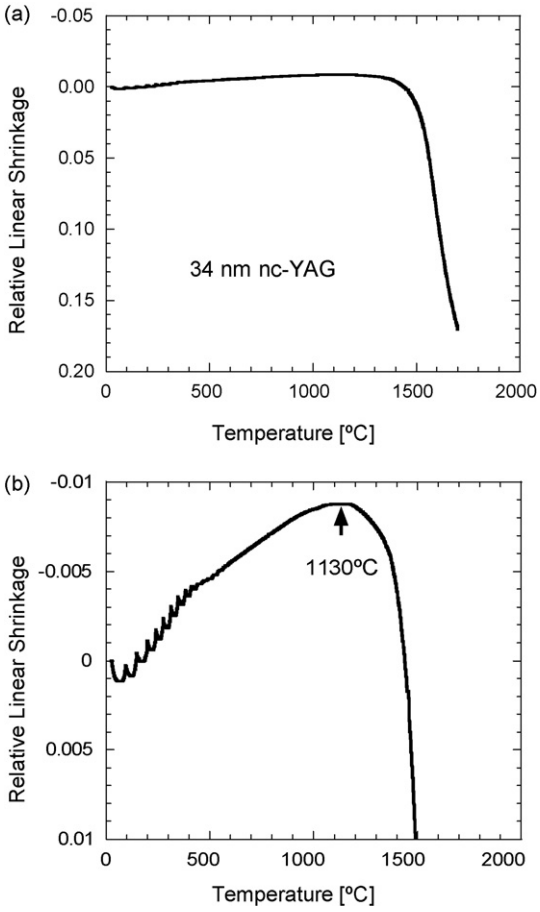

Fig. 3. Dilatometric linear shrinkage curves of the nc-YAG powder compact at the heating rate of 15 °C/min. (a) Relative linear shrinkages of 17% was recorded at 1700 °C. (b) The onset temperature of 1130 °C where the shrinkage starts is shown by the arrow.

this specimen was also log-normal with mean grain size of 87 ± 27 nm indicating on some grain coarsening. However, the nanocrystalline character of the powder did not assist densification to full density at such low temperature without applied pressure.

The microstructures at higher SPS temperatures were also remarkably homogeneous whether in porous opaque specimens sintered at 1250 °C (Fig. 5a) or in dense transparent specimens with equiaxed polyhedral-shape (tetrakaidekahedra) grains fabricated at 1400 °C (Fig. 5b). The relative density and the mean grain size versus the SPS temperatures are shown in Fig. 6 and summarized in Table 1. Significant increase in the relative density (from 83 to 99.6%) was observed within the narrow temperature range of 150 °C, between 1250 and 1400 °C. The corresponding grain size in this temperature range increased with temperature in a parabolic manner and tended to saturation in the submicrometer range. However, significant grain growth was observed at the SPS temperatures above 1400 °C, where the grain size grew to a few micrometers. It is of noteworthy that the two different grain growth behaviors follow the two different density ranges below and above 1400 °C (Fig. 6). This observation will further be discussed below.

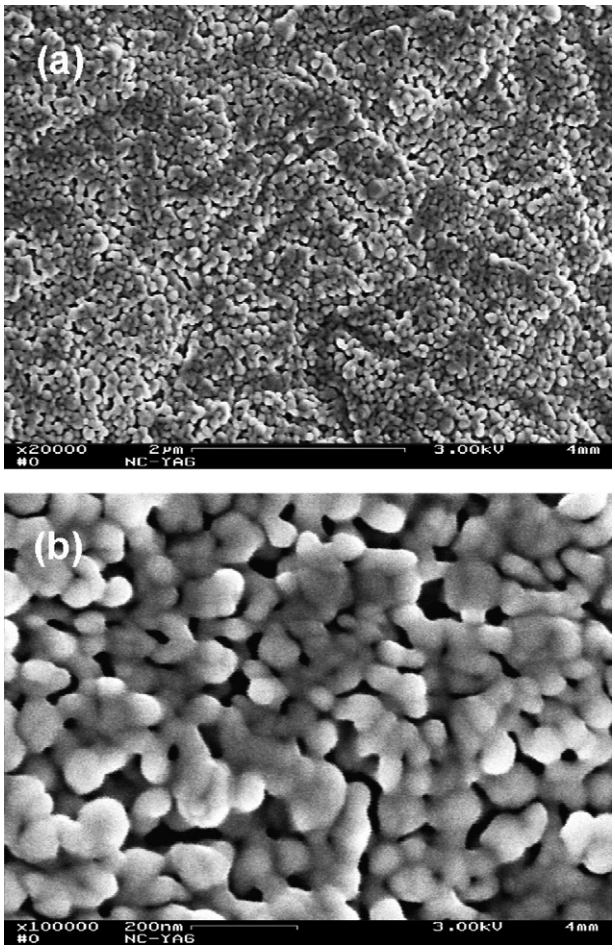

Fig. 4. (a) Low and (b) high magnification HRSEM images from the nc-YAG compact subjected to SPS for 3 min at 900 °C and 100 MPa, and further annealed for 5 h at 900 °C. The homogeneous distribution of the particles and pores with comparable sizes are visible.

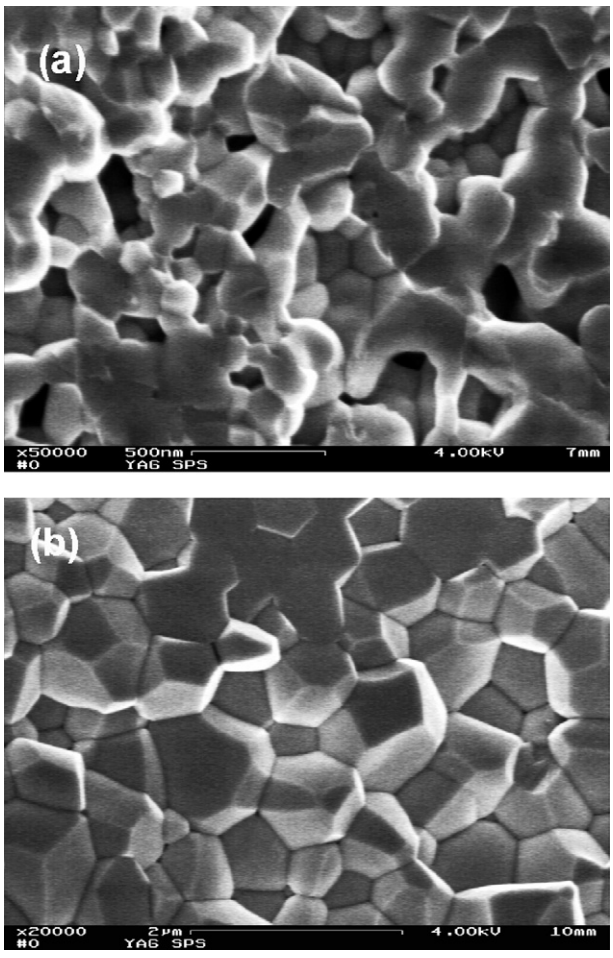

Fig. 5. HRSEM images of nc-YAG fracture surfaces after SPS for 3 min at 100 MPa and (a) 1250 °C; (b) 1450 °C.

3.3. Effect of SPS duration

The effect of the SPS duration on the densification and grain growth was evaluated using different durations of 3, 6, and 9 min. Significant increase was found in the relative density with increase in the SPS duration from 3 to 6 min, especially at the lower temperature range, below 1300 °C (Fig. 7). For a given relative density in this temperature range, the SPS temperature may be lowered by ~75 °C while increasing the SPS duration from 3 to 6 min. Nevertheless, the resultant density after 6 min at 1300 °C was still low for which the opacity of the specimen was unchanged (specimens 2 and 8 in Table 1). Consequently, 6 min sintering at the higher temperature 1350 °C was needed to reach fully dense specimens with optical transparency (specimen 9 in Table 1). The fact that higher density was observed for 6 min at 1300 °C compared to 3 min at 1350 °C (Fig. 7) indicates on the detrimental effect of the grain growth on densification during the SPS. This implies that the densification mechanism is associated with the atomic transport processes at the particle surfaces and their interfaces. This effect is very important and should be taken into account in the SPS temperature–time cycle plan, for densification rate optimization.

HRSEM images from the specimens after 3 and 6 min SPS at 1400 °C are shown in Fig. 8. In some instances, internal microstructure within large grains was observed (Fig. 8b) indicating on densification by grain boundary sliding and rotation.

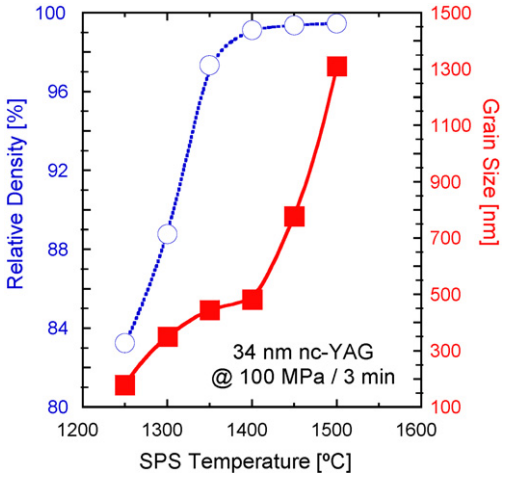

Fig. 6. Relative density (circles) and mean grain size versus the SPS temperature at 100 MPa for 3 min duration. Two grain growth regimes above and below 1400 °C were observed.

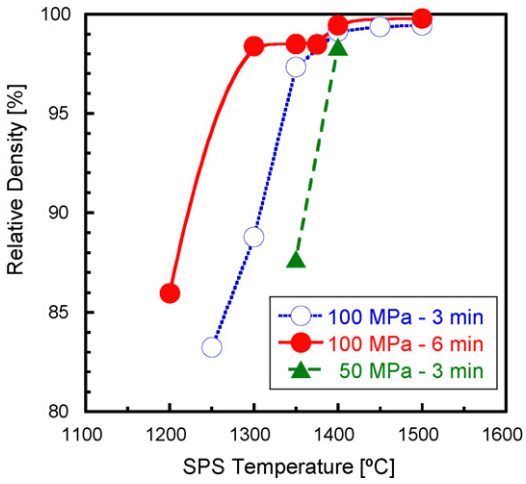

Fig. 7. Relative density of the nc-YAG powder compact after SPS for 3 and 6 min at 50 and 100 MPa and the respective temperatures.

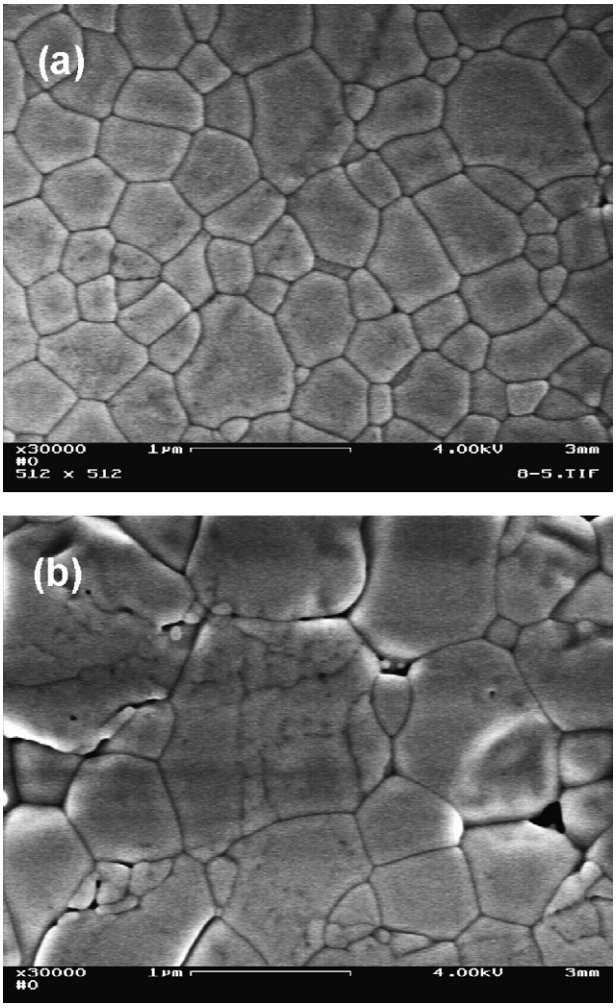

Fig. 8. HRSEM images from the thermally etched surfaces of YAG specimens subjected to SPS at 1400 °C and 100 MPa for different durations. (a) 3 min; (b) 6 min. The internal nano-grain clusters within the larger grain in (b) demonstrate the densification mechanism by nano-grain rotation and sliding.

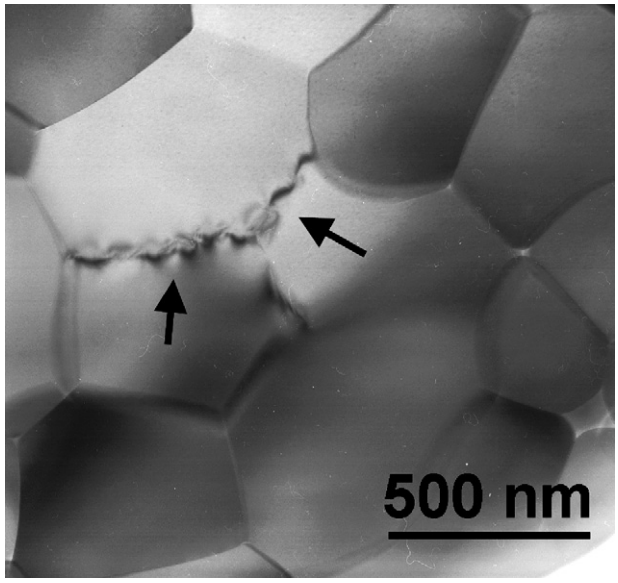

Fig. 9. TEM image of the nc-YAG subjected to SPS for 3 min at 1400 °C and 100 MPa. The high angle grain boundaries appear as straight lines. The low-angle grain boundaries (arrowed) appear curvy due to the dislocations strain field. Nanometer size residual pores are present at the grain boundary junctions.

Densification and grain growth by grain rotation and sliding is expected to convert the originally high angle grain boundaries (HAGB's) to low angle grain boundaries (LAGB's) that in turn are annealed out by short circuit diffusion. TEM observations verified the presence of such LAGB's in the dense specimens (Fig. 9). At the shorter SPS durations, when the grains are in the submicron size range (Fig. 8a) densification may still be efficient by grain boundary sliding. Nevertheless, at longer SPS durations, where the grains are in the micrometer range (Fig. 8b) further densification by grain boundary sliding is much difficult and may result in residual pores which can be annealed out only by grain boundary diffusion for prolong durations. The increase in the residual pore size may be responsible for the loss of transparency at the higher SPS temperatures and durations, as can be deduced from Table 1.

3.4. Effect of SPS pressure

The effect of the SPS pressure was evaluated by decreasing the SPS pressure from 100 to 50 MPa for two experiments at 1350 and 1400 °C (specimens 3 and 4 versus 13 and 14 in Table 1). No significant changes were observed in the relative density (Fig. 7) and transparency (Table 1) compared to the specimen fabricated under 100 MPa at 1400 °C. However decrease by 50 °C in the SPS temperature (i.e. to 1350 °C) has led to significant decrease in the final density (from 97.33 to 87.69%). This finding may indicate on strong temperature dependence of the grain boundary viscous shear strength. The grain boundary shear strength is expected to increase (exponentially) with temperature decrease hence lower densities are expected at lower temperatures compared to the specimens fabricated at 100 MPa.

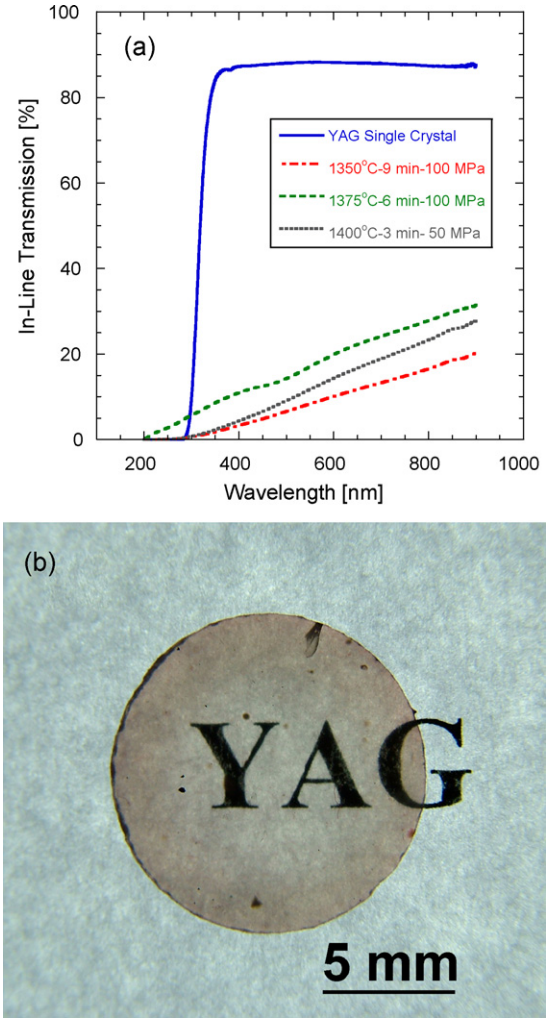

Fig. 10. (a) In-line transmission spectra in the visible range of YAG specimens fabricated at different SPS conditions. (b) The optical transparency of the 0.5 mm thick disc fabricated for 3 min at 1400 °C and 100 MPa is demonstrated.

3.5. Optical transparency

The in-line transmission in the visible range of selected specimens fabricated at different SPS conditions and the reference YAG single crystal were shown in Fig. 10. The single crystal YAG with isotropic refraction index of 1.8245 (at 800 nm) should transmit more than 90% of the incident intensity.[13] The observed 88% in-line transmission from the single crystal is in accordance with theoretical expectation. It is evident, that despite the good visual transparency of the present specimens (Fig. 10b) the measured transmitted intensity is between 6 to 14% at the green (500 nm) and increases to 20–32% at 900 nm. The lower transmitted intensity at the lower wavelengths originates from the higher Rayleigh scattering in this range, the scattered intensity being inversely proportional to the fourth power of the wavelength.[14] The residual nano-size pores observed in the sintered microstructure most probably are the main cause for the strong scattering of light. Nevertheless, removal of these pores necessitates long term annealing in vacuum and is not expected to be achievable within the time frame of a few minutes during the SPS.

4. Discussion

It is of noteworthy that the two different grain growth behaviors followed the two different density ranges below and above 1400 °C (Fig. 6). Generally, such difference in the grain growth behavior is explained in terms of the nature of the porosity as following. Slow grain growth may be expected at low relative densities (below ~90%) where continuous pores act as efficient obstacles to the grain boundary migration. At higher densities, the pores become isolated and located along the grain boundaries and at the grain junctions. The isolated pores may also pin the grain boundary if the pore mobility is lower than the grain boundary mobility. Recent investigations have shown that the mobility of the triple junctions is important as much as that of the grain boundaries in determining the grain growth kinetics.[15,16] However, rapid grain growth is expected in practically fully dense specimens where a few isolated pores may be present only at the grain boundary triple junctions. Although closed pores may still be present at temperatures above1400 °C, the mobility of the triple junctions is expected to increase with temperature. In such a scenario, normal grain growth, with grain growth exponent $n=2$ should dominate over the entire temperature range (1250–1500 °C) indicating a single grain boundary diffusion mechanism, i.e. curvature driven grain growth. Detailed grain growth analysis of the present data has shown two different grain growth mechanisms below and above 1400 °C.[17] Normal grain growth, controlled by grain boundary diffusion of Y^{3+} was determined only above 1400 °C. The calculated grain growth exponent $n=2$ and the corresponding activation energy $Q=553$ kJ/mol were in excellent agreement with the grain growth data for dense YAG fibers.[18] On the other hand, grain growth below 1400 °C yielded grain growth exponent $n=3$ and activation energy 435 kJ/mol that correspond to volume diffusion through the liquid phase layer. Formation of a liquid phase was suggested during the SPS[19] but was not verified due to its transient nature during the process. However, formation of a few large YAG crystals within residual cavities formed by evaporation–condensation mechanism indicated on the presence of a liquid phase during the SPS.[17] The diffusion coefficients and the activation energies derived from the grain growth analyses supported the presence of the liquid at various stages of densification.

The interplay between the various SPS parameters (temperature, duration, pressure) is a projection of the densification mechanisms mentioned above. First, it was manifested in the observed densities with respect to SPS temperature and duration. Consequently lower temperatures and longer durations are preferable for full densification by SPS, provided the later parameter is short enough compared to the diffusion durations needed for conventional hot pressing. Lower SPS temperatures may limit the particle coarsening, but yet high enough to permit densification by grain boundary rotation and sliding. Increased coarsening lowers the density of the available interfaces needed for densification through the

latter process. At the same conditions, threshold SPS pressure is needed to overcome the shear strength of the grain boundaries. As densification and grain growth accelerated with temperature, the effect of pressure becomes marginal due to the loss of the free surfaces (pores) and interfaces (grain boundaries) that were associated with the densification mechanisms.

The resultant grain morphology of tetrakaidekahedra with planar (non-curved) grain boundaries resembles equilibrium shape grains, the further grain growth of which may need diffusion processes for long durations. Therefore, removal of the isolated nanosize pores found at the grain boundary junctions may be kinetically impossible within the SPS time frame. Consequently, the resultant dense specimens may be partially transparent as was shown above.

5. Summary and conclusions

It was found that full densification of pure nc-YAG necessitates application of threshold stress and optimal temperature where the densification rate is maximal and the respective grain growth rate is minimal. In this respect superfast densification to fully dense transparent YAG was achieved by SPS for 3 min at 100 MPa and 1375 °C. The densification mechanism deduced from the microstructural observation was nano-grain rotation and sliding, most probably aided by partial melting of the particles surfaces. The grain growth was associated with densification of the nano-grain clusters in hierarchy with respect to their size. At higher densities normal grain growth takes place with curvature driven grain boundary migration. Since the densification rate decreases with grain growth and thus with SPS duration, residual closed pores are an inevitable feature of the microstructure left after the SPS. Consequently, theoretical full density needed for ideal optical transparency may not be achieved within the time frame of a few minutes of the SPS process.

Acknowledgments

The financial supports by the Ministry of Defense and the Fund for Promotion of Research at the Technion are gratefully acknowledged. Dr. Gitti Frey is acknowledged for providing the optical facilities.

References

1. Cheng, J., Agrawal, D., Zhang, Y. and Roy, R., Microwave sintering of transparent alumina. *Mater. Lett.*, 2002, **56**, 587–592.
2. Krell, A., Blank, P., Ma, H., Hutzler, T., Van Bruggen, M. P. B. and Apetz, R., Transparent sintered corundum with high hardness and strength. *J. Am.Ceram. Soc.*, 2003, **86**, 12–18.
3. Wu, Y. J., Kimura, R., Uekawa, N., Kakegawa, K. and Sasaki, Y., Spark plasma sintering of transparent $PbZrO_3$–$PbTiO_3$–$Pb(Zn_{1/3}Nb_{2/3})O_3$ ceramics. *Jpn. J. Appl. Phys.*, 2002, **41**, L219–L221.
4. Xiong, Y., Fu, Z. Y. and Wang, H., Microstructural effects on the transmittance of transparent AlN ceramics by SPS. *Mater. Sci. Eng. B*, 2006, **128**, 7–10.
5. Chaim, R., Shen, Z. and Nygren, M., Transparent nanocrystalline MgO by rapid and low-temperature spark plasma sintering. *J. Mater. Res.*, 2004, **19**, 2527–2531.
6. Ikegami, T., Matsuda, Sh. I. and Suzuki, H., Effect of halide dopants on fabrication of transparent polycrystalline MgO. *J. Am. Ceram. Soc.*, 1974, **57**, 507–1507.
7. Sekita, M., Haneda, H., Shirasaki, S. and Yanagitani, T., Optical spectra of undoped and rare-earth—(=Pr, Nd, Eu, and Er) doped transparent ceramic $Y_3Al_5O_{12}$. *J. Appl. Phys.*, 1991, **69**, 3709–3718.
8. Ikesue, A., Polycrystalline Nd:YAG ceramics lasers. *Opt. Mater.*, 2002, **19**, 183–187.
9. Lu, J., Ueda, K. I., Yagi, K., Yanagitani, T., Akiyama, Y. and Kaminskii, A. A., Neodymium doped yttrium aluminum garnet ($Y_3Al_5O_{12}$) nanocrystalline ceramics—a new generation of solid state laser and optical materials. *J. Alloys Compd.*, 2002, **341**, 220–225.
10. Chaim, R. and Margulis, M., Densification maps for spark plasma sintering of nanocrystalline MgO ceramics. *Mater. Sci. Eng. A*, 2005, **407**, 180–187.
11. Chaim, R., Densification mechanisms in spark plasma sintering of nanocrystalline ceramics. *Mater. Sci. Eng. A*, 2007, **443**, 25–32.
12. Marcel, J., John, T., Baranwal, R., Hinklin, T. and Laine, R., Yttrium aluminum garnet nanopowders produced by liquid-feed flame spray pyrolysis (LF-FSP) of metalloorganic precursors. *Chem. Mater.*, 2004, **16**, 822–831.
13. Kingery, W. D., Bowen, H. K. and Uhlmann, D. R., *Introduction to Ceramics*. Wiley, New York, 1976 (Chapter 13).
14. Tilley, R., *Colour and the Optical Properties of Materials*. Wiley, Chichester, 2000 (Chapter 5).
15. Gottstein, G., Ma, Y. and Shvindlerman, L. S., Triple junction motion and grain microstructure evolution. *Acta Mater.*, 2005, **53**, 1535–1544.
16. Mattissen, D., Molodov, D. A., Shvindlerman, L. S. and Gottstein, G., Drag effect of triple junctions on grain boundary and grain growth kinetics in aluminum. *Acta Mater.*, 2005, **53**, 2049–2057.
17. Chaim, R., Marder-Jaeckel, R. and Shen, J. Z., Transparent YAG ceramics by surface softening of nanoparticles in spark plasma sintering. *Mater. Sci. Eng. A*, 2006, **429**, 74–78.
18. King, B. H. and Halloran, J., Polycrystalline yttrium aluminum garnet fibers from colloidal sols. *J. Am. Ceram. Soc.*, 1995, **78**, 2141–2148.
19. Tokita, M., Mechanism of spark plasma sintering and its application to ceramics. *Nyu Seramikkusu (New Ceramics)*, 1997, **10**, 43–53 (in Japanese).